Superconducting Hydride Mg_2RhH_6 Experimentally Achieved at Lower Pressure

Linjing Wu [a §], Zelong Wang [a §], Guiqi Liu [a §], Jun Zhang [a *], Yanfeng Ge [b], Yuanhao Su [a], Runteng Chen [a], Hongyu Liu [a], Wenmin Li [c], Sijia Zhang [a], Jingcheng Zhu [a], Jianfa Zhao [a], Zheng Deng [a], Shaomin Feng [a], Jing Song [a], Qingqing Liu [a], Xiang Li [d], Haozhe Liu [e], Panpan Kong [a *], Xiancheng Wang [a] and Changqing Jin [a,f *]

[a] *Beijing National Laboratory for Condensed Matter Physics, Institute of Physics, Chinese Academy of Sciences, Beijing,100190, China.*

[b] *State Key Laboratory of Metastable Materials Science and Technology & Hebei Key Laboratory of Microstructural Material Physics, School of Science, Yanshan University, Qinhuangdao, 066004, China.*

[c] *Institute of Quantum Materials and Physics, Henan Academy of Sciences, Zhengzhou 450046, China.*

[d] *Centre for Quantum Physics, Key Laboratory of Advanced Optoelectronic Quantum Architecture and Measurement (MOE), School of Physics, Beijing Institute of Technology, Beijing 100081, China.*

[e] *Center for High Pressure Science & Technology Advanced Research, Beijing, 100094, China.*

[f] *School of Physics, University of Chinese Academy of Sciences, Beijing 100190, China.*

* Email: zhang@iphy.ac.cn

* Email: panpankong@iphy.ac.cn

* Email: jin@iphy.ac.cn

§ Linjing Wu, Zelong Wang and Guiqi Liu contributed equally to this work.

Abstract

Although tremendous progress has been made in recent years in the field of polyhydride superconductors, the realization of high critical temperature (T_c) superconductivity still relies on formidable high pressures. Searching for superconducting hydrides at lower pressures is of particular importance. Here we report the first experimental synthesis of Mg_2RhH_6, which exhibits superconductivity under a significantly reduced pressure of 30 GPa. The synthesis of Mg_2RhH_6 proceeds via a two-step process: (1) preparing the Mg_2RhH_5 precursor, in which hydrogen atoms are stabilized by covalent bonds, and (2) introducing additional hydrogen, which injects electrons into antibonding orbitals above 30 GPa and simultaneously triggers a structural transition from RhH_5 square pyramids to RhH_6 octahedra. Superconductivity emerges at ~30 GPa with a T_c of 24 K, and the T_c is further enhanced to 29 K upon synthesis at 53 GPa, as evidenced by a sharp drop to zero resistivity and the characteristic suppression of T_c under applied magnetic fields. Our results demonstrate that Mg_2RhH_6 is thermodynamically stable above 30 GPa, establishing it as the first superconductor with a T_c of approximately 30 K at a readily accessible pressure. This study pioneers a highly promising pathway for the rational design and discovery of high-temperature superconductors within the phonon-mediated BCS framework.

Introduction

Hydrogen-rich materials have long been considered potential candidates for high-temperature superconductivity within the phonon-mediated BCS framework, due to the high Debye vibration mode of the lightest element hydrogen. In 1968, Ashcroft proposed that metallic hydrogen might be superconducting with a high superconducting critical temperature (T_c) under extremely high-pressure conditions [1]. However, for a long time thereafter, little significant progress was made. In 2004, a novel approach termed "chemical pre-compression" was proposed to achieve hydrogen metallization [2]. By compressing hydrogen-rich compounds, this approach enables the realization of hydrogen metallization and high-temperature superconductivity at relatively low pressures [2]. Subsequently, hydrogen-rich materials, such as SiH_4 [3] and GeH_4 [4], have become a focus of both theoretical and experimental investigations. A landmark compound, H_3S, was initially predicted to be a superconductor with a T_c of approximately 205 K [5]. Subsequently, an experiment quickly confirmed a superconducting transition with a T_c of 203 K in H_3S at ~150 GPa [6]. This finding validated the "chemical pre-compression" theory and accelerated the development of the conventional phonon-mediated hydrogen-based superconductors.

Based on the "chemical pre-compression" theory, numerous binary hydrogen-based superconductors have been designed and have demonstrated high T_cs in recent years. Rare earth hydrides (e.g. LaH_{10}, T_c = 252 K at 170 GPa [7]; YH_6, T_c = 220 K at 183 GPa [8] and YH_9, T_c = 243 K at 201 GPa [8]) and alkaline earth metal hydrides (such as CaH_6, T_c = 200 K at 160 GPa, 215 K at 172 GPa [9-10]) feature metal atoms with electronegativity significantly lower than that of hydrogen, leading to the formation of hydrogen clathrate structures with predominantly ionic bonding. In contrast, covalent-type hydrogen-rich superconductors like H_3S (T_c = 203 K at 150 GPa) [6], SbH_4 (T_c = 116 K at 184 GPa) [11] exhibit primarily covalent bonding under high pressure. Transition metal hydrides, such as ZrH_6 (T_c = 71 K at 220 GPa) [12], HfH_{14} (T_c = 83 K at 243 GPa) [13], NbH_3 (T_c = 42 K at 187 GPa) [14] and TaH_3 (T_c = 30 K at 197 GPa) [15] have been experimentally discovered and stretched hydrogen molecules exist in these materials. Owing to the ultra-high pressures (> 150 GPa) compression, the

distance between hydrogen atoms in such materials is relatively small. Taking solid metallic hydrogen as an example, theory predicts that the hydrogen-hydrogen distance ($d_{(H-H)}$) approaches 1 Å at 500 GPa [1].

The core proposition of chemical pre-compression for achieving high-temperature superconductivity involves filling hydrogen's antibonding orbitals with electrons from non-hydrogen elements. This enables density of states of hydrogen to contribute to the Fermi surface. The filling of electrons into antibonding orbitals results in a repulsive interaction in hydride superconductors. Generally, ultra-high pressures are required to enhance the filling of hydrogen's antibonding orbitals, stabilize the structure and achieve a high superconducting T_c. Although the T_cs of typical hydrides, including H_3S ($d_{(H-H)}$ = 1.5 Å, T_c = 203 K at 150 GPa) [6], LaH_{10} ($d_{(H-H)}$ = 1.1 Å, T_c = 252 K at 170 GPa) [7, 16], YH_9 ($d_{(H-H)}$ = 1.1 Å, T_c = 243 K at 201 GPa)[8], CaH_6 ($d_{(H-H)}$ = 1.2 Å, T_c = 200 K at 160 GPa, 215 K at 172 GPa)[9-10] have approached room temperature due to the large contribution of hydrogen states at the Fermi surface and strong electron phonon coupling (EPC), the ultra high pressures required hinder the investigations into some physical phenomena and the superconductivity mechanism, such as the Meissner effect. To address this issue, strategies such as chemical doping and covalent stabilization have been explored to reduce the pressures required for achieving superconducting states in hydrogen-rich compounds. For example, the lowest stable pressure for $La_{1-x}Ce_xH_{9-10}$ was reported to be about 100 GPa with a T_c of 176 K [17]. However, these approaches often result in a concurrent decrease in the T_c (LaH_{10}, T_c = 252 K at 170 GPa) [7]. Further theoretical studies have predicted a series of multi-component hydrides capable of achieving high T_c under low pressures, such as $LaBH_8$ with a T_c of 156 K at 55 GPa [18], $LaBeH_8$ with a T_c of 98 K at 185 GPa [19]. A later experiment confirmed that $LaBeH_8$ exhibits superconductiviting T_c of 110 K under 80 GPa [20].

To further reduce the pressure required for preparing a new hydride superconductor, we propose that covalent bonding between hydrogen and transition metals with similar electronegativity can stabilize hydrogen atoms at an appropriate distance from each other. Further electron doping fills the antibonding orbitals of both the transition metal and hydrogen, enabling their density of states to contribute to the

Fermi surface. Theoretically, this approach can reduce the pressure required for hydrides to obtain superconducting properties. The electronegativity of the noble metals is very close to that of hydrogen, making noble metal hydrides a proper system to validate our proposal [21]. Recently, multiple independent research groups have conducted theoretical investigations on ternary hydrides Mg_2XH_6 (where X = noble metal), exhibiting remarkably high T_cs ranging from 45 K to 80 K [22-26] and even one prediction reaching as high as 160 K for Mg_2IrH_6 [24-27]. Thermodynamic stability and EPC strength calculations show that Mg_2MH_6 (M = Rh and Ir) is metastable under ambient pressure and has a high possibility of being synthesized [25, 27]. Usually, the stable transition metal complexes obey the 18 valence electron rule under ambient pressure conditions. Mg_2MH_6 (M = Ir and Rh) has 19 valence electrons, while Mg_2IrH_5 and Mg_2RhH_5 obey the 18-electron rule and therefore should be more thermodynamically stable under ambient pressure conditions. For instance, a series of compounds adhering to the 18-electron rule - namely Mg_2FeH_6 [28], Mg_2CoH_5 [29], and Mg_2NiH_4 [30], have all been successfully synthesized and are stable under ambient conditions. More recently, Mg_2IrH_5 was stabilized at ambient pressure [31] and further Mg_2IrH_7 near 40 GPa [32], while the synthesis of Mg_2MH_6 (M = Rh, Ir) has not yet been achieved.

Motivated by the interest of the Mg_2Ir/RhH_6 system, theoretical studies have designed several preparation routes. These routes primarily involve the initial synthesis of either Mg_2IrH_5, which has 5/6 hydrogen site occupancy in the IrH_6 octahedra [31] or Mg_2IrH_7, which has an additional interstitial non-bonding hydrogen atom located at the edge center of the cubic crystal [27], followed by hydrogen insertion or removal. Also, hydrogenating Mg_2IrH_5 to form Mg_2IrH_6 with the *Amm*2 polymorph was proposed, which is slightly more stable than the $Fm\bar{3}m$ phase at low pressure [27]. Usually, the calculations are performed at zero temperature and Mg_2Ir/RhH_6 is predicted to be metastable under ambient pressure [24-25]. The pressurization effect can, to some extent, be equated with lowering the temperature. Therefore, Mg_2Ir/RhH_6 might be preserved to room temperature when an appropriate pressure is applied.

Mg_2IrH_5 with a *P*4/*nmm* structure and an identical metallic sublattice is exceptionally close to the predicted high-T_c superconductor Mg_2IrH_6. Only a single

hydrogen atom needs to be added per formula unit to obtain the superconducting phase. Calculations of kinetic barrier indicates that the Mg_2IrH_5 (*P4/nmm*) system smoothly transitions to the face-centered cubic (fcc) Mg_2IrH_6 structure without any energey barrier [31]. Based on the aforementioned ideas, we propose a two-step synthesis method: (1) Synthesis of tetragonal Mg_2Ir/RhH_5. Given the close electronegativity between Ir (2.20)/Rh (2.28) and H (2.20), the synthesis of Mg_2Ir/RhH_5 can utilize the covalent interaction between Ir/Rh and H to stabilize hydrogen atoms at an appropriate distance (~2.2 Å) [21]. (2) Supplementing hydrogen to prepare the Mg_2Ir/RhH_6. Hydrogen injection under pressure-temperature conditions can achieve electron filling into the antibonding orbitals of Ir/Rh and H, potentially enabling their density of states to contribute to the Fermi surface and inducing a superconducting phase transition. Based on sample synthesis, comprehensive structural and electrical property measurements were carried out. The synthesized Mg_2RhH_6 sample exhibited a maximum T_c of 29 K, while the synthesis of Mg_2IrH_6 is still in progress.

Experimental part

Polycrystalline samples of Mg_2RhH_5 (*P4/nmm*) were prepared by a high-pressure and high-temperature route using a 6 × 1400 T cubic anvil high pressure apparatus. Commercially available crystalline powders of MgH_2 (Alfa, 99.9% pure), Rh (Alfa, 99.99% pure) and ammonia borane (NH_3BH_3) (Alfa, 97% pure) were used as starting materials. The MgH_2 and Rh powders were mixed in a stoichiometric ratio of 2:1 and thoroughly ground, then pressed into a pellet. NH_3BH_3 and the mixture were placed in a "sandwich-like configuration" in a sealed Au cylinder and sintered at 900 ℃ under 6 GPa for 30 min to obtain pure polycrystalline samples.

Powder samples of Mg_2RhH_6 were prepared by a two-step synthesis route, including first synthesizing Mg_2RhH_5 (*P4/nmm*) under high pressure conditions and then achieving an additional hydrogen insertion at high pressures by laser heating to 1000-1800 K. NH_3BH_3 served as the hydrogen source. The initial pressure, calibrated by the ruby fluorescence method, was set in the range of 30-70 GPa. Different synthesis conditions were attempted, such as pressure, laser power, duration and

number of heating cycles. Multiple laser heating spots were distributed across the sample chamber to improve the temperature uniformity for synthesizing Mg_2RhH_6 samples. Additionally, dual-sided laser heating was routinely employed to minimize thermal gradients. Temperatures were calibrated spectroradiometrically and monitored in situ via resistance measurements. Reaction completion was confirmed by the stabilization of resistance during iterative heating. The detailed synthesis conditions are summarized in Table SI in the Supporting Information. The nine prepared diamond anvil cell (DAC) samples, labeled as Samples 1-9# were used for transport property measurements. The XRD data were collected based on Sample 10#.

Powder X-ray diffraction (XRD) measurements were carried out on a Rigaku Smart Lab diffractometer with Cu *K*α radiation (λ = 1.54059 Å, 45 kV, 200 mA) in the 2θ range of 4 - 100° with a step size of 0.01°. The diffraction spectra were refined by EXPGUI software [33]. Raman spectra were recorded using a 532 nm laser for excitation. The spectra covered the range of 100–3200 cm^{-1} with a spectral resolution of 1 cm^{-1}, employing an integrated Renishaw Raman system equipped with a confocal microscope and a multichannel air-cooled CCD detector. The electronic transport properties were measured by four-probe electrical conductivity methods in a MagLab system with temperatures varying from 300 to 2 K and a magnetic field up to 7 T. The DAC technique was employed for generating high pressure. The beveled diamonds with 300/100 μm culets were chosen and T301 stainless steel was used as the gasket; a mixture of aluminum oxide, sodium chloride, and epoxy resin served as the insulating layer and ammonia borane powder served as the pressure-transmitting medium and hydrogen source. The electric current was set to 0.1 mA during the resistance measurement. The pressure was calibrated by the ruby fluorescence method. The synchrotron radiation XRD experiments under high pressure conditions were performed at the Shanghai Synchrotron Radiation Facility with a radiation wavelength of 0.6199 Å using a symmetric DAC at room temperature. The details of in situ high-pressure experiments can be seen in Refs [11, 34-35].

Results

Crystal structure analysis. As to the synthesized polycrystalline sample of Mg_2RhH_5, XRD measurements were carried out with Cu *K*α radiation in the 2θ range from 4° to 100° with a step size of 0.01°. All reflections can be indexed on a tetragonal lattice, as shown in Figure 1(a). The structure refinement was carried out by adopting the initial structural model of Mg_2CoH_5 with the space group of *P4/nmm* reported by Zolliker [36], which smoothly converged with χ^2 = 5.24, wRp = 3.73%, Rp = 2.48% and confirmed the high quality of our sample. The lattice constants are *a* = *b* = 4.6164(0) Å, *c* = 6.8233(1) Å and unit cell volume (*V*) of 145.41(0) Å^3 when *Z*=2. Based on the refinement results, a drawing of the main structural unit of Mg_2RhH_5 is shown in Figure 2(a-b). Tetragonal Mg_2RhH_5 (denoted as Mg_2RhH_5-T below) exhibits a distorted CaF_2-type metal atom structure and is mainly composed of five-coordinate rhodium (RhH_5^{4-}) in an ordered square-pyramidal configuration and Mg^{2+} ions. A C_{4V} symmetry exists in the RhH_5^{4-} unit. The crystallographic data and selected interatomic distances for Mg_2RhH_5-T are summarized in Table SII. As expected for a d^8 system of this symmetry, the metal-ligand distances toward the base (1.5583(1) Å) are significantly shorter than those toward the apex (1.7256(0) Å), and the bond angle of $\angle H_1$-Rh-H_1 is 170.657(1)°. The Rh-H bond lengths are consistent with covalent bonding interactions. The Rh atom is displaced by 0.13 Å from the square pyramidal base toward the apex. The distances of $d_{(H1-H1)}$ and $d_{(H1-H2)}$ within the square pyramidal structure of Mg_2RhH_5-T are 2.1964(8) Å and 2.4174(6) Å, respectively.

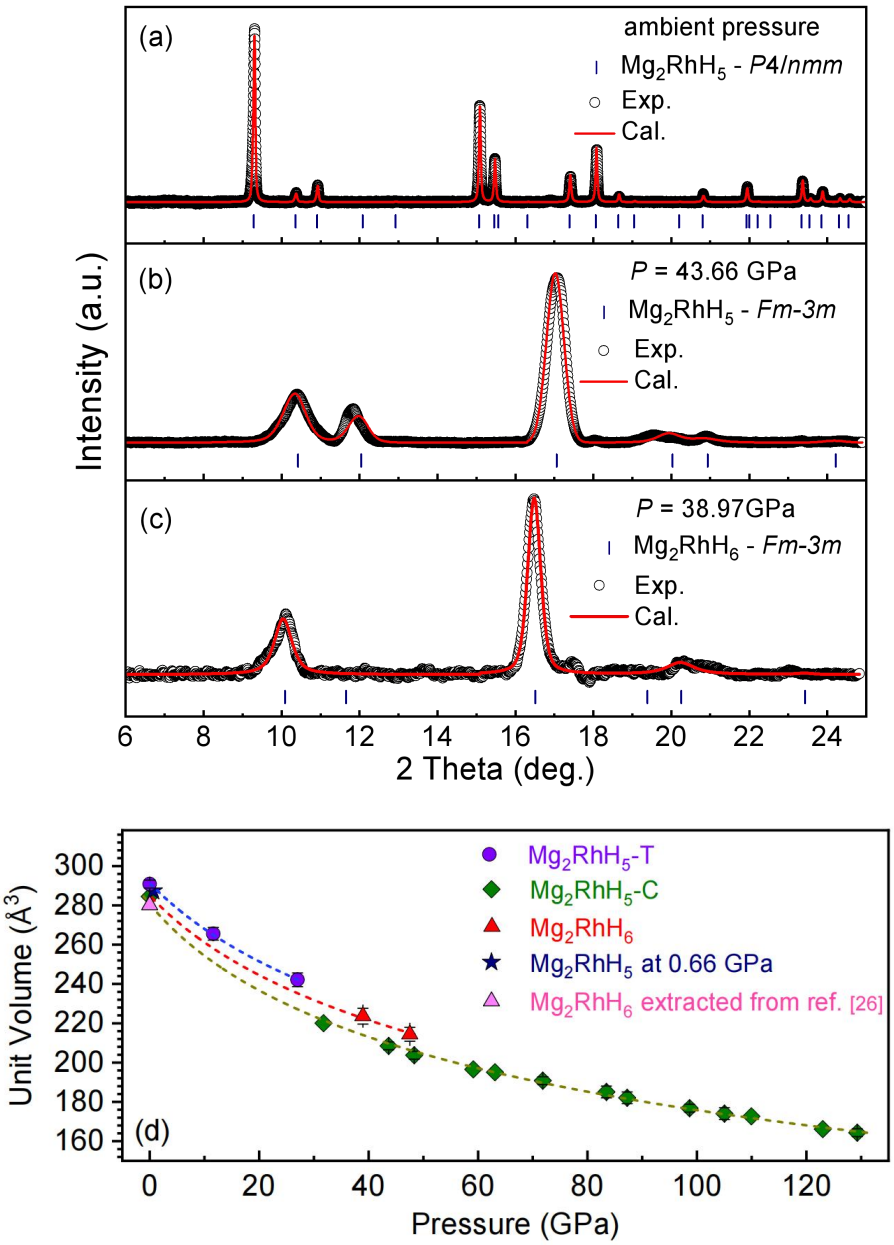

Figure 1 (a-c) Powder XRD data (represented by circles) and corresponding Rietveld refinement (represented by red lines) for three samples: Mg_2RhH_5-T (measured at ambient pressure), Mg_2RhH_5 ($Fm\bar{3}m$, denoted as Mg_2RhH_5-C and measured at 43.66 GPa) and Mg_2RhH_6 ($Fm\bar{3}m$, measured at 38.97 GPa). The structural data of Mg_2RhH_5-T were collected using Cu *K*α radiation (λ =1.54059 Å) and then converted to synchrotron radiation data (λ = 0.6199 Å) for better comparison with high pressure data. Vertical line bars in the figure mark the positions corresponding to different phases. (d) The pressure and volume relationship for Mg_2RhH_5-T, Mg_2RhH_5-C and Mg_2RhH_6. A phase transition from Mg_2RhH_5-T to Mg_2RhH_5-C occurred above 30 GPa. Mg_2RhH_6 was synthesized from Mg_2RhH_5-T using a hydrogen

source using DAC equipment at 38.97 GPa after heating to 1000 K. The recovered Mg_2RhH_5, obtained by decompressing the Mg_2RhH_6 sample synthesized at 38.97 GPa, was measured at 0.66 GPa. Unit-cell volume data are also included. The pressure - volume data are fitted with a second-order Birch-Murnaghan equation of state (EoS) as shown by the dashed lines.

Theoretical calculations predicted that Mg_2IrH_6 can be obtained from isostructural Mg_2IrH_5 or Mg_2IrH_7 by adjusting the hydrogen content [27, 31]. Experimental verification is still lacking. The plausible reason is that this phase may be more metastable rather than thermodynamically stable at ambient pressure and room temperature, and therefore can only be quenched through some non-equilibrium methods. In addition, the tetragonal structure of Mg_2CoH_5 can be easily transformed into a disordered cubic structure at ~480 K [36], which is almost isostructural with the theoretically predicted Mg_2MH_6 (M= noble metal) [24]. Considering the similar effects of pressure and temperature in the material synthesis, a structural transition under high pressure is also expected. The structure changes of Mg_2RhH_5-T under high pressure are investigated. As can be seen from Figure S1, all peaks broaden and systematically shift to higher angles compared with those at ambient pressure as the pressure increases to 27 GPa. An obvious structural transition is observed at 31.76 GPa although the tetragonal structure partially remains as the (111) and (002) peaks of the cubic phase are still asymmetric. When the pressure is further enhanced, the diffraction peaks of (112) and (020) merge and evolve into a cubic structure. These peaks can be well fitted, as shown in Figure 1(b). The crystal lattice is consistently compressed as the pressure is increased to 130 GPa. No new peak appears, which indicates that the crystal structure of Mg_2RhH_5 ($Fm\bar{3}m$, denoted as Mg_2RhH_5-C below) remains stable in this pressure region.

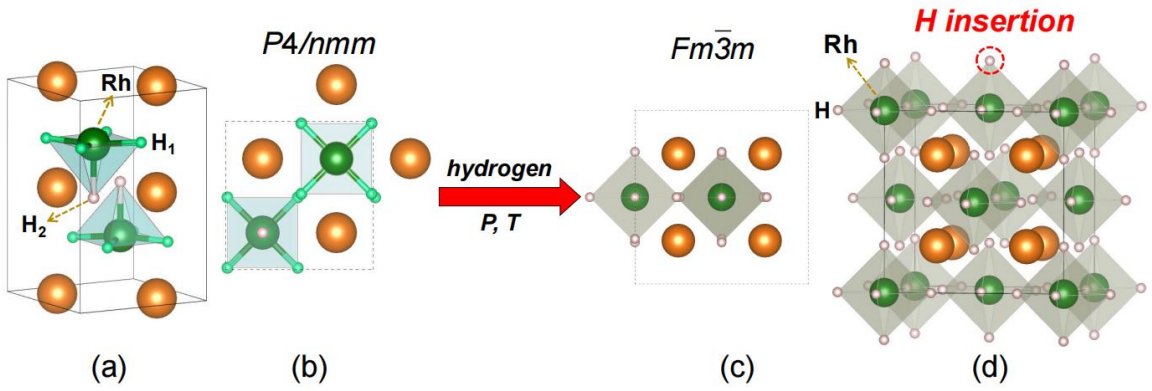

Figure 2 (a-b) Crystal structure sketches and coordination environment of Rh in Mg_2RhH_5 (*P4/nmm*). The Rh ions are in a square-pyramidal configuration, with four H_1 atoms in the basal plane and one H_2 atom at the apex. (c-d) Crystal structure sketches and coordination environment of Rh in Mg_2RhH_6 ($Fm\bar{3}m$), where Rh ions are coordinated by six H atoms forming an ideal octahedral configuration.

All the diffraction data of Mg_2RhH_5 were refined, and the typical refinement patterns are shown in Figure S2. Figure 1(d) shows the pressure-volume relationship. At a pressure of 30 GPa, there is an abrupt decrease, indicating a first-order phase transition. That is, tetragonal Mg_2RhH_5 with RhH_5^{4-} square-pyramidal configuration transforms to cubic Mg_2RhH_5. The Mg_2RhH_5-C consists of RhH_6^{4-} octahedra but has a hydrogen occupancy of 5/6 on the octahedral sites. Here, the phase transition is similar to that reported in Mg_2CoH_5 [36]. Further compression leads to a smooth reduction in volume. The Birch-Murnaghan equation was used to deduce the bulk modulus B_0. The dashed lines are the fitted results obtained with the second-order Birch equation of state (EoS):

$$P(GPa)=\frac{3}{2}\times B_0\left[(V_0/V)^{\frac{7}{3}}-(V_0/V)^{\frac{5}{3}}\right]\times\left\{1-\left(3-\frac{3}{4}\times B_0^{'}\right)\times\left[(V_0/V)^{\frac{2}{3}}-1\right]\right\}$$

where the pressure derivative $B_{0'}$ is set as 4, a fitting to the data up to 27 GPa gives the bulk modulus B_0 = 101.19(1) GPa, V_0= 291.35(0) Å^3 for Mg_2RhH_5-T, whereas a fitting to the data with pressure up to 130 GPa gives B_0 = 83.50(7) GPa, V_0 = 280.66(4) Å^3 for Mg_2RhH_5-C.

Bond stretching/bending frequencies are sensitive to the local coordination environment, providing a diagnostic probe for distinguishing different molecular complexes. We measured Raman spectra of tetragonal Mg_2RhH_5 and by comparison with Mg_2IrH_5 [31], observed similar vibrational peaks (Figure S3). However, the stretching mode of Rh–H at ~2200 cm^{-1} severely overlaps with the diamond peak as pressure increased to 15 GPa, making it unresolvable. We thus tracked the Raman peak evolution at 717 cm^{-1} and 1936 cm^{-1} under pressure. As shown in Figure S3(c), an obvious change near 30 GPa corroborates the XRD-detected phase transition from tetragonal to cubic phase. The phase transition is accompanied by the evolution from a RhH_5^{4-} square pyramid to a disordered RhH_6^{4-} octahedron with one hydrogen vacancy.

An attempt was made to prepare Mg_2RhH_6 under high pressure conditions where a phase transition was observed. By combining laser heating for hydrogen insertion, it was expected to successfully prepare the target compound. Mg_2RhH_5-T and NH_3BH_3 (serving as a hydrogen source) were used as the starting materials and the initial pressure was set to 43 GPa. After heating at ~1000 K, the pressure in the DAC for Sample $10^{\#}$ was monitored and calibrated to be 38.97 GPa. The crystal structure was inspected using a synchrotron radiation source with a wavelength of 0.6199 Å. As can be seen from Figure 1(c), the diffraction patterns after heating became very simple, with only two distinct peaks observed. By comparing the diffraction patterns with those of Mg_2RhH_5-C at 43.66 GPa in Figure 1(b), the crystal structure can be indexed as the cubic phase of Mg_2RhH_x, where x depends on the stoichiometry. After careful refinement, the unit cell volumes at different pressures are shown in Figure 1(d), where the volume curve representing Mg_2RhH_x lies above that of Mg_2RhH_5-C. It is well known that determining the hydrogen content in the newly synthesized hydrogen-based superconductors, particularly those prepared by high pressure techniques, remains challenging. Alternatively, as reported in previous studies on metal hydrides, the formation of a metal hydride is typically accompanied by volume expansion relative to the pure metal lattice, owing to hydrogen incorporation. The volume increase upon hydrogenation ranges from 2-3 $Å^3$ [37]. After careful examination, the volume expands by ~2.4(0) $Å^3$ per Mg_2RhH_x unit compared with Mg_2RhH_5-C at

38.97 GPa. This result indicates that Mg_2RhH_6, the theoretically predicted high-temperature superconductor, may have been synthesized. Equation of state fitting yields a bulk modulus B_0 = 96.13(2) GPa, V_0= 285.02(0) Å^3. Furthermore, Raman spectroscopic measurements, shown in Figure S3, revealed a distinct vibrational mode at around 423 cm^{-1} for the sample containing Mg_2RhH_5 and NH_3BH_3 after heating at 45.09 GPa. This mode is in good agreement with the T_{2g} vibrational mode of $[IrH_6]^{4-}$ reported in Ref. [32], providing consistent evidence for the formation of Mg_2RhH_6.

Superconductivity property investigations. The electrical resistance of the Mg_2RhH_5-T sample under pressure was first measured, as shown in Figure S4. Mg_2RhH_5-T exhibits semiconducting behavior at ambient pressure, which agrees with the calculated results for tetragonal phase Mg_2IrH_5 [31]. As pressure increases to ~30 GPa, the electrical resistance sharply decreases to 1.3 Ω at room temperature, and further compression persistently reduces the resistance. The high-pressure XRD patterns in Figure S1 clearly reveal a structural transition from the tetragonal to the cubic phase for Mg_2RhH_5-T above ~30 GPa. This transformation is further supported by (i) characteristic changes in the Rh–H vibrational modes, evolving from square-pyramidal RhH_5^{4-} to octahedral RhH_6^{4-} in the Raman spectrum (Figure S3), and (ii) the distinct drop in electrical resistance near ~30 GPa. The sample remains semiconducting up to 54.44 GPa. Therefore, Mg_2RhH_5-C with a disordered hydrogen occupation is concluded to be a semiconductor in this pressure range, consistent with the predicted result for cubic Mg_2IrH_5 [31].

Hydrogen insertion is expected to induce a metallic phase in Mg_2RhH_6. A sample (designated Sample 4$^{\#}$) was synthesized at 55 GPa. Electrical resistance measurements were performed to confirm the superconducting transition in Mg_2RhH_6. As shown in Figure 3(a), zero resistance is observed in both warming and cooling runs. The T_c, determined from the onset of the dR/dT peak, is ~18 K (inset of Figure 3(a)). Notably, residual semiconducting behavior persists in the vicinity of the superconducting transition. The evolution of superconducting transitions under magnetic fields is shown in Figure 3(b), where superconductivity is gradually suppressed to lower temperatures as the field increases to 4 T. This provides solid

evidence for superconductivity in Mg_2RhH_6.

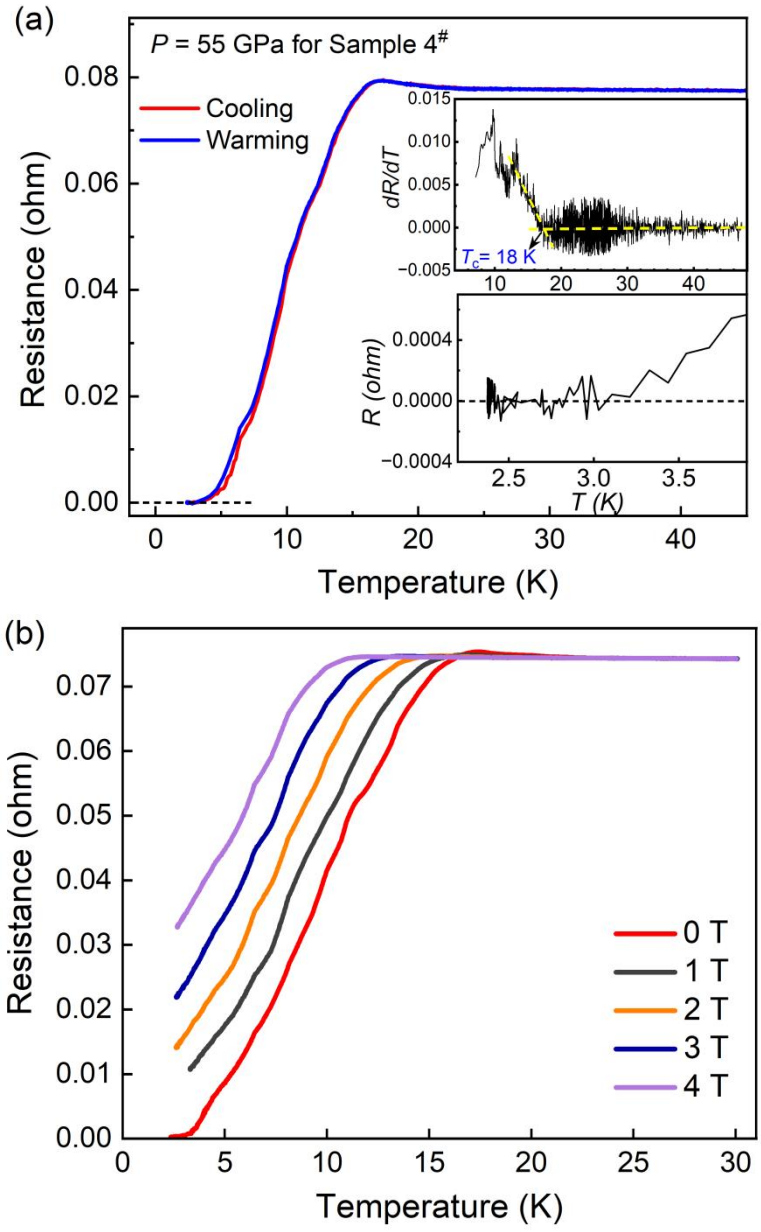

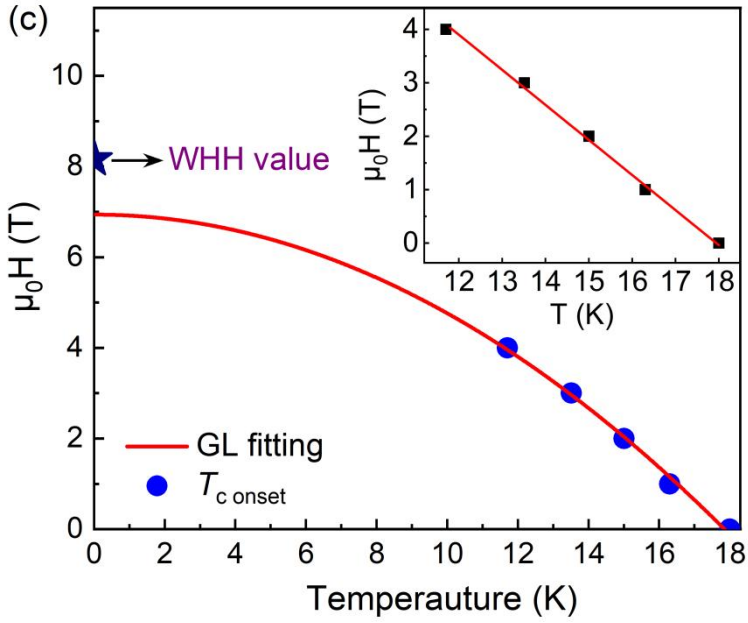

Figure 3 (a) The temperature-dependent resistance of the Sample 4# measured at 55 GPa during the warming and cooling process. The inset shows the derivative of resistivity (dR/dT) as a function of temperature under zero magnetic field. The superconducting transition temperature can be determined from the turning point of the dR/dT curve. The zero-resistance state is achieved with a residual resistance lower than ±0.0002 Ω, comparable to the instrument noise level. (b) Resistance curves of the Sample 4# measured at 55 GPa under different magnetic fields. (c) The Ginzburg-Landau fitting for the H_{c2}(T) is shown by the red solid lines. The star denotes the H_{c2}(0) value calculated via the WHH model. The inset shows the upper critical field H_{c2}(T) as a function of temperature.

The superconducting parameters, including upper critical field H_{c2}(0) and Ginzburg-Landau (GL) coherence length ξ, are determined from the measurements on Sample 4#. The $T_{c\ onset}$ under magnetic field ranging from 0 to 4 T is determined using criteria based on the resistance derivative with respect to temperature (dR/dT). The temperature dependence of critical field H_{c2} is shown in the inset of Figure 3(c). Linear fitting yields a slope of $dH_{c2}/dT|_{Tc}$ = −0.657 T/K for the criteria of $T_{c\ onset}$. Using the Werthamer-Helfand-Hohenberg (WHH) formula, μ_0H_{c2}(T) = -0.69 × dH_{c2}/dT|$_{Tc}$ × T_c, the H_{c2}(0) value was calculated to be 8.16 T. The GL formula, μ_0H_{c2}(T) = μ_0H_{c2}(0) ×(1-(T/T_c)^2) was also used to estimate the H_{c2}(0) at zero temperature. As shown in Figure 3(c), fitting μ_0H_{c2}(T) with the GL formula yields H_{c2}(0) = 6.94 T. Furthermore, the GL coherence length ξ was estimated to be 6.35–6.89 Å using the relation μ_0H_{c2}(0)

= $\Phi_0/2\pi\xi^2$, where Φ_0 = 2.067 × 10^{-15} Web is the magnetic flux quantum and $H_{c2}(0)$ = 6.94–8.16 T from WHH and GL fits. Additionally, high-field electrical transport measurements with magnetic field up to 7 T were performed on Sample 9# (Figure S5). The $\mu_0 H_{c2}(0)$ value obtained from the WHH formula is 9.63 T, which is close to our estimates obtained from Sample 4#.

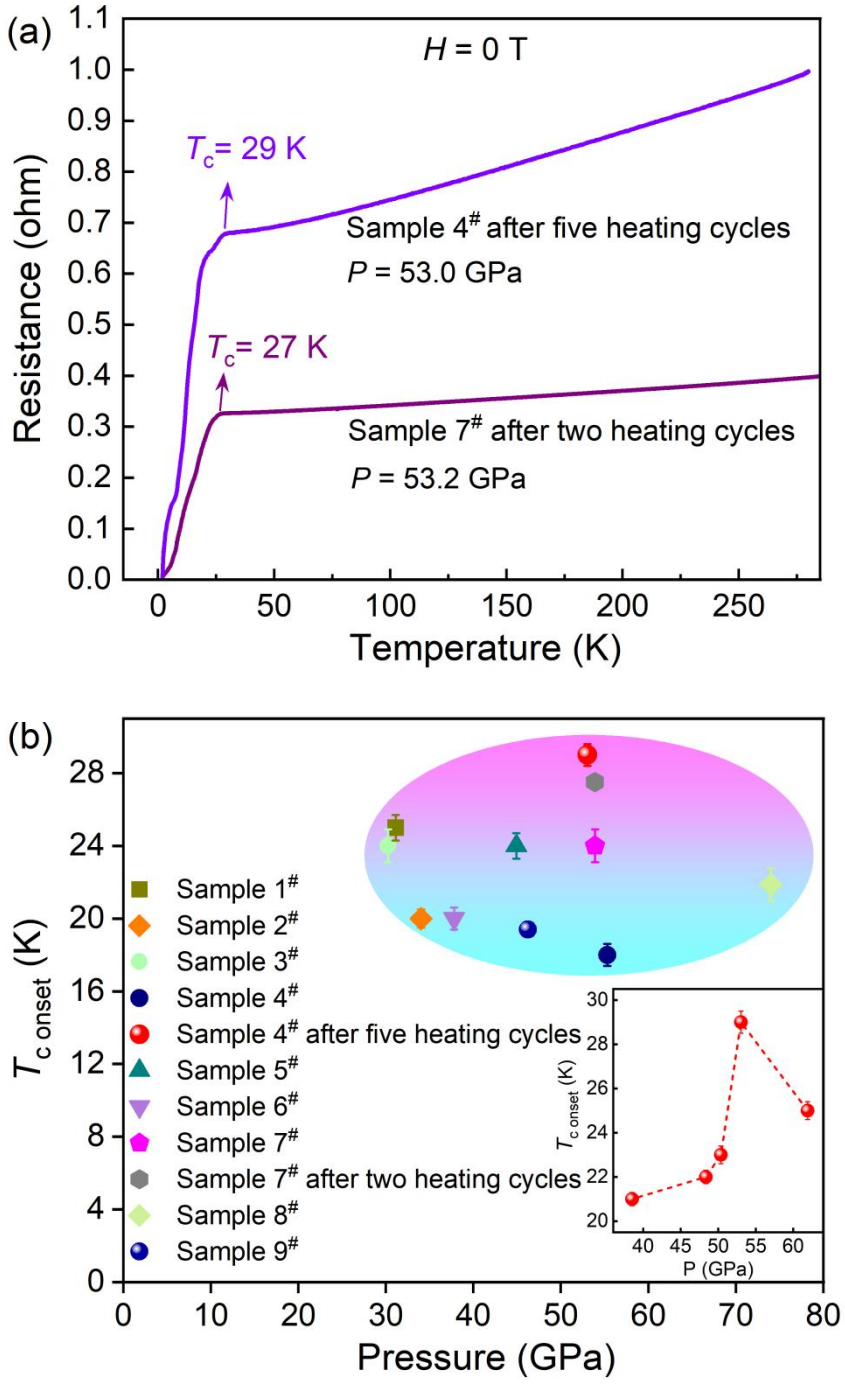

Figure 4 Superconducting transitions determined by electrical resistance measurements. (a) Temperature dependence of the electrical resistance measured in the cooling process for Sample 4# and Sample 7# within the temperature range of 2-285 K after multiple heating

cycles at high pressure. The arrow indicates the superconducting transition and T_c. (b) The pressure dependence of the $T_{c\ onset}$ for Mg_2RhH_6 samples (Sample 1-9#) synthesized at 30-74 GPa. The inset shows the T_c evolution upon decompression for the Sample 4# after five heating cycles.

To improve the sample homogeneity of Mg_2RhH_6 and enhance the superconducting transition temperature, a series of synthesis experiments were performed, including the preparation of Samples 1-9# at 30-74 GPa, followed by heating to 1000-1800K. Figure 4(a) shows the temperature dependence of the resistance for Sample 4# after five heating cycles, measured during cooling. Metallic behavior is observed in the temperature range from 29 K to room temperature, consistent with the predicted behavior. The resistance quickly drops near 29 K, as indicated by the arrow and approaches zero at low temperatures, suggesting that a superconducting transition occurs in this Mg_2RhH_6 sample. A fully metallic normal state and a superconducting transition at 27 K were also observed in sample 7# synthesized at 53.2 GPa after two heating cycles. In contrast, the cubic Mg_2RhH_5 still exhibits semiconducting behavior up to 54.44 GPa (Figure S4). This clear distinction further confirms the successful synthesis of the theoretically predicted superconducting Mg_2RhH_6 phase.

Figure S6 shows the typical resistance measurements for samples synthesized under various pressure conditions, and details of Samples 1-9# are summarized in Table SI. The drops in electrical resistance are all observed for samples prepared under pressures of 30-74 GPa. For example, Sample 1# exhibits an obvious turning point in electrical resistance at 25 K under 31 GPa, while Sample 8# shows a turning point at 22 K under 74 GPa. Figure 4(b) shows the onset temperatures of the superconducting transition as a function of synthesis pressure (30-74 GPa) for Samples 1-9#, demonstrating intrinsic superconductivity in Mg_2RhH_6 with T_c values ranging from 18 to 29 K. The irregular variations in T_c with synthesis pressure are closely associated with hydrogen deficiencies in Mg_2RhH_{6-x} since the introduction of hydrogen atoms serves as electron doping, which dominates the density of states near the Fermi surface and thus T_c. Several theoretical studies have predicted T_c

values in the range of 45 - 59 K for Mg_2RhH_6 [24-26], consistent with our estimated value of ~60 K at 30 - 50 GPa by first-principles calculations (Table SIII), while the experimentally observed maximum T_c in our work is ~29 K. The discrepancy arises from two main factors: (i) variations in the computational methodologies employed in different theoretical works, and (ii) sample inhomogeneities inherent to the high-pressure DAC synthesis technique. In our experiments, the multiple heating cycles result in a gradual increase in T_c. We attribute this primarily to the improved sample homogeneity, especially the improvement of inherent hydrogen nonstoichiometry at grain boundaries in the synthesized polycrystalline Mg_2RhH_6 samples.

High-pressure AC magnetic susceptibility measurements are highly desirable for observing distinct diamagnetic shielding signals, yet this technique remains challenging within a diamond anvil cell owing to the tiny sample volume and a substantial diamagnetic background signal from the gasket and the cell body. Nevertheless, our extensive transport measurements show excellent reproducibility across multiple runs, and in situ XRD and Raman spectra confirm structural stability. Although the absolute shielding fraction cannot be quantified, these consistent results strongly support the intrinsic superconducting phase of the synthesized Mg_2RhH_6 sample.

Decompression investigations. Theoretical predictions suggest that the Mg_2RhH_6 superconductor is thermodynamically metastable under ambient pressure [24-25]. To investigate this, we conducted decompression experiments on Sample 4#. As shown in Figure S7, at 53.02 GPa the material exhibits a superconducting T_c of 29 K. Upon further compression to 61.91 GPa, T_c decreases to 25 K. During the subsequent decompression, T_c gradually declines—for instance, at 38.51 GPa, it drops to 21 K. When the pressure is reduced to 28.34 GPa, the temperature dependence of the electrical resistance indicates an insulator-to-metal phase transition. As the pressure is further reduced to near-ambient levels, the material becomes completely insulating, consistent with the behavior of Mg_2IrH_5 with 5/6 hydrogen occupation. XRD measurements were performed on the Mg_2RhH_6 sample synthesized at 38.97 GPa after full decompression. As shown in Figure S8, the pattern collected from the

recovered product at 0.66 GPa can be well refined using the cubic structure of Mg_2RhH_5 (space group *Fm*-3*m*), with the excellent refinement parameters of $\chi^2 = 0.59$, wRp = 9.92%, and Rp = 7.34%. The refined lattice constant a = 6.5907(1) Å and unit-cell volume V = 286.28(2) Å^3 are in good agreement with the experimental values of a = 6.5772(0) Å and V = 284.52(7) Å^3 for our independently synthesized cubic Mg_2RhH_5, which is a stable phase at ambient pressure as reported for the sister compound Mg_2IrH_5 [31-32].

Discussion

Structure stability. Theoretically, Mg_2RhH_6 is predicted to be metastable under ambient pressure, with a formation energy lying ~30 meV above the convex hull [26]. However, our high-pressure structural and electrical transport property measurements confirm that Mg_2RhH_6 decomposes into semiconducting Mg_2RhH_5 upon decompression below 30 GPa. Based on these results, we suggest that Mg_2RhH_6 should be thermodynamically stable only above 30 GPa, which is supported by the negative formation enthalpy and phonon dispersion spectra obtained from calculations above 30 GPa (Figure S9). Furthermore, the experimental results show that Mg_2RhH_6 can be synthesized at 30-60 GPa, yet further increasing the synthesis pressure does not enhance its T_c. As reported in recent literature [32], Mg_2IrH_5 converts directly into Mg_2IrH_7 (rather than the theoretically predicted Mg_2IrH_6) under high synthesis pressure above 40 GPa with laser heating. It is plausible that Mg_2RhH_6 can be synthesized only within a finite high pressure range.

Superconductivity mechanism. Mg_2RhH_6 adopts a fcc structure, in which the RhH_6^{4-} units form ideal octahedra. These octahedra are entirely isolated from one another, and the shortest hydrogen-hydrogen distance, $d_{(H-H)}$, which occurs between adjacent RhH_6^{4-} octahedra, measures 2.0601(3) Å at a pressure of 38.97 GPa (a = 6.0697(1) Å, V = 223.61(6) Å^3). The distance represents a compression of approximately 7.77 % compared with the ambient pressures (where $d_{(H-H)}$ = 2.2336(6) Å, a = 6.5809(7) Å, V_0 = 285.02(0) Å^3, V_0 derived from equation-of-state fitting). Concurrently, the Rh-H distance decreases from 1.7110(5) Å to 1.5781(2) Å under compression. Notably, despite this reduction, the $d_{(H-H)}$ value in Mg_2RhH_6 remains significantly larger than those reported in other ionic (e.g. $d_{(H-H)}$ ~1.2 Å in CaH_6 [9]), covalent (e.g. $d_{(H-H)}$ ~1.5 Å in

H_3S [5]), and transition-metal-based hydrogen-rich superconducting materials (e.g. $d_{(H-H)}$ ~ 0.9 Å in HfH_{14} [13]). Furthermore, it is worth mentioning that the radius of hydrogen ions typically ranges from 1.4 to 2.1 Å [37-38], implying a minimum distance between hydrogen ions of approximately 2.8 Å. This is considerably larger than the observed $d_{(H-H)}$ value of 2.0601(3) Å in Mg_2RhH_6 at 38.97 GPa. Moreover, the Rh-H distance of 1.5781(2) Å at this pressure is characteristic of covalent bonding. These observations together suggest the presence of covalent interactions not only between adjacent hydrogen atoms but also between the central metal Rh and its coordinated hydrogen atoms in Mg_2RhH_6. Therefore, the superconductivity observed in Mg_2RhH_6 may not be exclusively governed by the density of states of hydrogen at the Fermi surface. As corroborated by theoretical calculations, the density of states near the Fermi level in Mg_2RhH_6 is primarily dominated by the e_g* antibonding states of the transition metals, which are hybridized with the H-1s and Mg-3s states [24]. This finding aligns with our hypothesis that electrons fill into antibonding orbitals of Rh and H atoms, thereby contributing to the electronic states at the Fermi level. In addition, the phonon linewidth in Mg_2RhH_6 is primarily contributed by H modes, which provide at least 2/3 of the integrated coupling constant λ as evidenced by previous theory work [25]. Recently, it was reported that BiH_2 exhibits superconductivity with a T_c of approximately 62 K under a pressure of 163 GPa. It was reported that covalent bismuth dominates the electronic states near the Fermi level, and contributes approximately 51% of the total λ [39]. For Mg_2RhH_6, the electronic states at the Fermi level are primarily derived from the transition metals, with their contributions significantly surpassing those from hydrogen and magnesium. These electronic states are likely to couple strongly with the high-energy vibrational modes of hydrogen atoms. The novel mechanism suggests the potential for achieving high T_c superconductivity in Mg_2RhH_6 based materials, warranting further theoretical exploration to elucidate the underlying physics and optimize material design.

Conclusion

In this study, we successfully synthesized the Mg_2RhH_6 hydride superconductor for the first time through a two-step route, demonstrating a maximum superconducting

T_c of up to 29 K under a pressure of 53 GPa. Our experimental results indicate that the cubic Mg_2RhH_6 is stabilized above ca. 30 GPa. The formation of strong covalent bonds between the noble metal (Rh) and hydrogen atoms stabilizes the hydride structure, while the subsequent injection of electrons into the antibonding orbitals induces superconductivity in this material. Further research, such as modifying the covalent bonds by substituting or alloying Rh with other precious metals, offers significant potential to achieve even higher T_c values at pressures closer to ambient conditions.

Supporting Information: Experimental details, including material synthesis, high pressure structure and resistance characterizations, decompression experiments and computational details of Mg_2RhH_5 and Mg_2RhH_6 (PDF).

Acknowledgements

This work was supported by the National Key R&D Program of China (Grant No. 2023YFA1406001, 2024YFA1408000, 2023YFA1608902 and 2022YFA1402301) and the National Natural Science Foundation of China (Grant No. 12474097, 12404164). We thank the staff members of the BL15U1 station (https://cstr.cn/31124.02.SSRFBL15U1) and User Experiment Assist System in Shanghai Synchrotron Radiation Facility (SSRF) (https://cstr.cn/31124.02.SSRF).

Reference:

1. Ashcroft, N. W., Metallic Hydrogen - A High-Temperature Superconductor. *Phys. Rev. Lett.* **1968,** *21* (26), 1748-1749.

2. Ashcroft, N. W., Hydrogen dominant metallic alloys: High temperature superconductors? *Phys. Rev. Lett.* **2004,** *92* (18), 187002.

3. Wang, S. B.; Mao, H. K.; Chen, X. J.; Mao, W. L., High pressure chemistry in the H_2-SiH_4 system. *Proc. Natl. Acad. Sci. U. S. A.* **2009,** *106* (35), 14763-14767.

4. Strobel, T. A.; Chen, X. J.; Somayazulu, M.; Hemley, R. J., Vibrational dynamics, intermolecular interactions, and compound formation in GeH_4-H_2 under pressure. *J. Chem. Phys.* **2010,** *133* (16), 164512.

5. Duan, D. F.; Liu, Y. X.; Tian, F. B.; Li, D.; Huang, X. L.; Zhao, Z. L.; Yu, H. Y.; Liu, B. B.; Tian, W. J.; Cui, T., Pressure-induced metallization of dense $(H_2S)H_2$ with high-superconductivity. *Sci. Rep.* **2014,** *4*, 6968.

6. Drozdov, A. P.; Eremets, M. I.; Troyan, I. A.; Ksenofontov, V.; Shylin, S. I., Conventional superconductivity at 203 kelvin at high pressures in the sulfur hydride system. *Nature* **2015,** *525* (7567), 73-76.

7. Drozdov, A. P.; Kong, P. P.; Minkov, V. S.; Besedin, S. P.; Kuzovnikov, M. A.; Mozaffari, S.; Balicas, L.; Balakirev, F. F.; Graf, D. E.; Prakapenka, V. B.; Greenberg, E.; Knyazev, D. A.; Tkacz, M.; Eremets, M. I., Superconductivity at 250 K in lanthanum hydride under high pressures. *Nature* **2019,** *569* (7757), 528-531.

8. Kong, P.; Minkov, V. S.; Kuzovnikov, M. A.; Drozdov, A. P.; Besedin, S. P.; Mozaffari, S.; Balicas, L.; Balakirev, F. F.; Prakapenka, V. B.; Chariton, S.; Knyazev, D. A.; Greenberg, E.; Eremets, M. I., Superconductivity up to 243 K in the yttrium-hydrogen system under high pressure. *Nat Commun* **2021,** *12* (1), 5075.

9. Li, Z. W.; He, X.; Zhang, C. L.; Wang, X. C.; Zhang, S. J.; Jia, Y. T.; Feng, S. M.; Lu, K.; Zhao, J. F.; Zhang, J.; Min, B. S.; Long, Y. W.; Yu, R. C.; Wang, L. H.; Ye, M. Y.; Zhang, Z. S.; Prakapenka, V.; Chariton, S.; Ginsberg, P. A.; Bass, J.; Yuan, S. H.; Liu, H. Z.; Jin, C. Q., Superconductivity above 200 K discovered in superhydrides of calcium. *Nat. Commun.* **2022,** *13* (1), 2863.

10. Ma, L.; Wang, K.; Xie, Y.; Yang, X.; Wang, Y. Y.; Zhou, M.; Liu, H. Y.; Yu, X. H.; Zhao, Y. S.; Wang, H. B.; Liu, G. T.; Ma, Y. M., High-Temperature Superconducting Phase in Clathrate Calcium Hydride CaH_6 up to 215 K at a Pressure of 172 GPa. *Phys. Rev. Lett.* **2022,** *128* (16), 167001.

11. Lu, K.; He, X.; Zhang, C. L.; Li, Z. W.; Zhang, S. J.; Min, B. S.; Zhang, J.; Zhao, J. F.; Shi, L. C.; Peng, Y.; Feng, S. M.; Liu, Q. Q.; Song, J.; Yu, R. C.; Wang, X. C.; Wang, Y.; Bykov, M.; Jin, C. Q., Superconductivity with of 116 K discovered in antimony polyhydrides. *National Science Review* **2024,** *11* (7), nwad241.

12. Zhang, C. L.; He, X.; Li, Z. W.; Zhang, S. J.; Feng, S. M.; Wang, X. C.; Yu, R. C.; Jin, C. Q., Superconductivity in zirconium polyhydrides with above 70 K. *Sci. Bull.* **2022,** *67* (9), 907-909.

13. Zhang, C.; He, X.; Li, Z.; Zhang, S.; Min, B.; Zhang, J.; Lu, K.; Zhao, J.; Shi, L.; Peng, Y.; Wang, X.; Feng, S.; Yu, R.; Wang, L.; Prakapenka, V. B.; Chariton, S.; Liu, H.; Jin, C.,

Superconductivity above 80 K in polyhydrides of hafnium. *Materials Today Physics* **2022,** *27*, 100826.

14. He, X.; Zhang, C.; Li, Z.; Lu, K.; Zhang, S.; Min, B.; Zhang, J.; Shi, L.; Feng, S.; Liu, Q.; Song, J.; Wang, X.; Peng, Y.; Wang, L.; Prakapenka, V. B.; Chariton, S.; Liu, H.; Jin, C., Superconductivity discovered in niobium polyhydride at high pressures. *Materials Today Physics* **2024,** *40*, 101298.

15. He, X.; Zhang, C. L.; Li, Z. W.; Zhang, S. J.; Min, B. S.; Zhang, J.; Lu, K.; Zhao, J. F.; Shi, L. C.; Peng, Y.; Wang, X. C.; Feng, S. M.; Song, J.; Wang, L. H.; Prakapenka, V. B.; Chariton, S.; Liu, H. Z.; Jin, C. Q., Superconductivity Observed in Tantalum Polyhydride at High Pressure. *Chin. Phys. Lett.* **2023,** *40* (5), 057404.

16. Liu, H. Y.; Naumov, I. I.; Hoffmann, R.; Ashcroft, N. W.; Hemley, R. J., Potential high-Tc superconducting lanthanum and yttrium hydrides at high pressure. *Proc. Natl. Acad. Sci. U. S. A.* **2017,** *114* (27), 6990-6995.

17. Chen, W. H.; Huang, X. L.; Semenok, D. V.; Chen, S.; Zhou, D.; Zhang, K. X.; Oganov, A. R.; Cui, T., Enhancement of superconducting properties in the La-Ce-H system at moderate pressures. *Nat. Commun.* **2023,** *14* (1), 2660.

18. Liang, X. W.; Bergara, A.; Wei, X. D.; Song, X. X.; Wang, L. Y.; Sun, R. X.; Liu, H. Y.; Hemley, R. J.; Wang, L.; Gao, G. Y.; Tian, Y. J., Prediction of high-Tc superconductivity in ternary lanthanum borohydrides. *Phys. Rev. B* **2021,** *104* (13), 134501.

19. Zhang, Z. H.; Cui, T.; Hutcheon, M. J.; Shipley, A. M.; Song, H.; Du, M. Y.; Kresin, V. Z.; Duan, D. F.; Pickard, C. J.; Yao, Y. S., Design Principles for High-Temperature Superconductors with a Hydrogen-Based Alloy Backbone at Moderate Pressure. *Phys. Rev. Lett.* **2022,** *128* (4), 047001.

20. Song, Y.; Bi, J.; Nakamoto, Y.; Shimizu, K.; Liu, H.; Zou, B.; Liu, G.; Wang, H.; Ma, Y., Stoichiometric Ternary Superhydride $LaBeH_8$ as a New Template for High-Temperature Superconductivity at 110 K under 80 GPa. *Phys. Rev. Lett.* **2023,** *130* (26), 266001.

21. Connor, N., Periodic Table of Elements. *https://www.periodic-table.org (2020-11-11)*.

22. Wang, X. Y.; Pickett, W. E.; Hutcheon, M.; Prasankumar, R. P.; Zurek, E., Why Mg_2IrH_6 Is Predicted to Be a High-Temperature Superconductor, But Ca_2IrH_6 Is Not. *Angew. Chem., Int. Ed.* **2024,** *63*, e202412687.

23. Luo, J.; Wei, Q.; Jia, X. F.; Zhang, M. G.; Zhu, X. M., First-principles study of high-temperature superconductivity in X_2MH_6 compounds under 20 GPa. *Supercond. Sci. Technol.* **2025,** *38* (5), 055005.

24. Zheng, F.; Zhang, Z.; Wu, Z.; Wu, S.; Lin, Q.; Wang, R.; Fang, Y.; Wang, C.-Z.; Antropov, V.; Sun, Y.; Ho, K.-M., Prediction of ambient pressure superconductivity in cubic ternary hydrides with MH_6 octahedra. *Materials Today Physics* **2024,** *42*, 101374.

25. Sanna, A.; Cerqueira, T. F. T.; Fang, Y.-W.; Errea, I.; Ludwig, A.; Marques, M. A. L., Prediction of ambient pressure conventional superconductivity above 80 K in hydride compounds. *npj Computational Materials* **2024,** *44* (10).

26. Cerqueira, T. F. T.; Fang, Y. W.; Errea, I.; Sanna, A.; Marques, M. A. L., Searching Materials Space for Hydride Superconductors at Ambient Pressure. *Adv. Funct. Mater.* **2024,** *34* (40), 2404043.

27. Dolui, K.; Conway, L. J.; Heil, C.; Strobel, T. A.; Prasankumar, R. P.; Pickard, C. J., Feasible Route to High-Temperature Ambient-Pressure Hydride Superconductivity. *Phys. Rev. Lett.* **2024,** *132* (16), 166001.

28. Didisheim, J. J.; Zolliker, P.; Yvon, K.; Fischer, P.; Schefer, J.; Gubelmann, M.; Williams, A. F., Dimagnesium Iron(II) Hydride, Mg_2FeH_6, Containing Octahedral FeH_6^{4-} Anions. *Inorg. Chem.* **1984,** *23* (13), 1953-1957.

29. Ivanov, E. J.; Konstanchuk, I.; Stepanov, A.; Jie, Y.; Pezat, M.; Darriet, B., The Ternary System Mg-Co-H. *Inorg. Chem.* **1989,** *28* (3), 613-615.

30. Yvon, K.; Schefer, J.; Stucki, F., Structural Studies of the Hydrogen Storage Material Mg_2NiH_4 1. Cubic High-Temperature Structure. *Inorg. Chem.* **1981,** *20* (9), 2776-2778.

31. Hansen, M. F.; Conway, L. J.; Dolui, K.; Heil, C.; Pickard, C. J.; Pakhomova, A.; Mezouar, M.; Kunz, M.; Prasankumar, R. P.; Strobel, T. A., Synthesis of Mg_2IrH_5: A potential pathway to high-Tc hydride superconductivity at ambient pressure. *Phys. Rev. B* **2024,** *110* (21).

32. Sinha, S.; Lu, W.; Hansen, M. F.; etc., High-pressure stabilization of Mg_2IrH_7: Structural proximity to high-T_c superconductivity. *2026-02-27, https://arxiv.org/abs/2602.23675v1*.

33. larson, A. C.; VON Dreele, R. B., General structure analysis system (GSAS). *Los alamos national laboratory report laur* **2000**, 86-748.

34. Zhang, C.; He, X.; Liu, C.; Li, Z.; Lu, K.; Zhang, S.; Feng, S.; Wang, X.; Peng, Y.; Long, Y.; Yu, R.; Wang, L.; Prakapenka, V.; Chariton, S.; Li, Q.; Liu, H.; Chen, C.; Jin, C., Record high T(c) element superconductivity achieved in titanium. *Nat. Commun.* **2022,** *13* (1), 5411.

35. Li, Z. W.; He, X.; Zhang, C. L.; Lu, K.; Min, B. S.; Zhang, J.; Zhang, S. J.; Zhao, J. F.; Shi, L. C.; Peng, Y.; Feng, S. M.; Deng, Z.; Song, J.; Liu, Q. Q.; Wang, X. C.; Yu, R. C.; Wang, L. H.; Li, Y. Z.; Bass, J. D.; Prakapenka, V.; Chariton, S.; Liu, H. Z.; Jin, C. Q., Superconductivity above 70 K observed in lutetium polyhydrides. *Sci China Phys. Mech.* **2023,** *66* (6), 267411

36. Zolliker, P.; Yvon, K.; Fischer, P.; Schefer, J., Dimagnesium Cobalt(I) Pentahydride, Mg_2CoH_5, Containing Square-Pyramidal CoH_5^{4-} Anions. *Inorg. Chem.* **1985,** *24* (24), 4177-4180.

37. Fukai, Y., The Metal-Hydrogen System. *Springer Series in Materials Science* **2005,** *21*.

38. Bouamrane, A.; Laval, J. P.; Soulie, J. P.; Bastide, J. P., Structural characterization of $NaMgH_2F$ and $NaMgH_3$. *Mater. Res. Bull.* **2000,** *35* (4), 545-549.

39. Ma, L.; Yang, X.; Li, M.; Shan, P. F.; Liu, Z. Y.; Hou, J.; Jiang, S.; Zhang, L. L.; Lin, C. L.; Yang, P. T.; Wang, B. S.; Sun, J. P.; Ding, Y.; Gou, H. Y.; Guo, H. Z.; Cheng, J. G., High Pressure Superconducting Transition in Dihydride BiH_2 with Bismuth Open-Channel Framework. *Phys. Rev. Lett.* **2025,** *135* (22), 226003.